

Phase-matched extreme-ultraviolet frequency-comb generation

Gil Porat^{1*}, Christoph M. Heyl^{1,2*}, Stephen B. Schoun^{1*}, Craig Benko¹,
Nadine Dörre³, Kristan L. Corwin^{1,4}, Jun Ye¹

¹JILA, NIST and the University of Colorado, 440 UCB, Boulder, Colorado 80309-0440, USA

²Department of Physics, Lund University, P.O. Box 118, SE-221 00 Lund, Sweden

³University of Vienna, Faculty of Physics, VCQ, Boltzmannngasse 5, A-1090 Vienna, Austria

⁴Department of Physics, Kansas State University, 116 Cardwell Hall, Manhattan, Kansas 66506, USA

*These authors contributed equally to this work.

Laser-driven high-order harmonic generation^{1,2} (HHG) provides tabletop sources of broadband extreme-ultraviolet (XUV) light with excellent spatial³ and temporal⁴ coherence. These sources are typically operated at low repetition rates, $f_{\text{rep}} \lesssim 100$ kHz, where phase-matched frequency conversion into the XUV is readily achieved^{5,6}. However, there are many applications that demand the improved counting statistics or frequency-comb precision afforded by operation at high repetition rates, $f_{\text{rep}} > 10$ MHz. Unfortunately, at such high f_{rep} , phase matching is prevented by the accumulated steady-state plasma in the generation volume^{7–11}, setting stringent limitations on the XUV average power. Here, we use gas mixtures at high temperatures as the generation medium to increase the translational velocity of the gas, thereby reducing the steady-state plasma in the laser focus. This allows phase-matched XUV emission inside a femtosecond enhancement cavity at a repetition rate of 77 MHz, enabling a record generated power of ~ 2 mW in a single harmonic order. This power scaling opens up many demanding applications, including XUV frequency-comb spectroscopy^{12,13} of few-electron atoms and ions for precision tests of fundamental physical laws and constants^{14–20}.

The highly-nonlinear HHG process requires peak laser intensities around 10^{14} W/cm², which necessitates large laser pulse energies $\gtrsim 10$ μ J, and short pulse durations $\lesssim 100$ fs, as typically reached with low repetition rate, chirped-pulse amplified²¹ laser systems. However, high repetition rates are desirable for applications such as photoelectron spectroscopy^{22–24} and microscopy²⁵ as well as electron-ion coincidence spectroscopy^{26,27}, which are limited by counting detection or space-charge effects to few XUV ionization events

per shot. Most notably, precision frequency-comb spectroscopy^{12,13} requires $f_{\text{rep}} \gg 10$ MHz in order to stabilize the comb. Recent efforts allowed HHG to be directly driven at $f_{\text{rep}} \gtrsim 1$ MHz, using either the direct output of a high-power oscillator^{22,28} or the coherent combination of several fibre amplifiers^{29,30}. Achieving the necessary intensity for HHG with $f_{\text{rep}} \gg 10$ MHz requires lasers with average power in the kW range. Apart from one demonstration at 20 MHz, where the measured XUV power was extremely low³¹, higher repetition rates up to 250 MHz³² have been facilitated only by using passive enhancement cavities, which store ~ 10 kW of laser power, where a gas jet is introduced at an intracavity focus^{7,10–12,33–35}.

In a macroscopic extended medium, efficient HHG requires matching the phase velocities of the generating laser and the generated fields. This can be achieved by balancing neutral and plasma dispersion, the geometric phase shift due to focusing (the Gouy phase), and the HHG intrinsic dipole phase^{5,36}. Achieving this balance becomes increasingly challenging as the repetition rate increases above ~ 10 MHz. The reason for this difficulty is that the plasma generated by one pulse does not have time to clear the focal volume before the next laser pulse arrives and generates even more plasma. Consequently, a high-density steady-state plasma is formed^{8,9}, which is highly dispersive (see Fig. 1a), making phase matching unattainable. While phase-matched HHG has been demonstrated at a repetition rate of 10.7 MHz²⁹, it has not been previously achieved at higher repetition rates, to the best of our knowledge.

Having identified the steady-state plasma as the main limitation for phase matching, we study its formation dynamics on the relevant time scale, which is the laser pulse repetition period $\tau_{\text{rep}} = 1/f_{\text{rep}}$. To this purpose, we define two dimensionless parameters: ξ_{ion} and ξ_{beam} , the number of laser pulses that enter the gas jet during the time it takes an ion to clear the ion-generation volume or during the transit time of an atom through the laser beam volume, respectively. The accumulation of plasma over many pulses stems directly from the intensity-dependent ξ_{ion} . However, in order to separate the highly-nonlinear intensity dependence of plasma accumulation from the effects of other experimental parameters, it is more convenient to use the intensity-independent parameter ξ_{beam} .

The precise definitions of ξ_{ion} and ξ_{beam} are as follows:

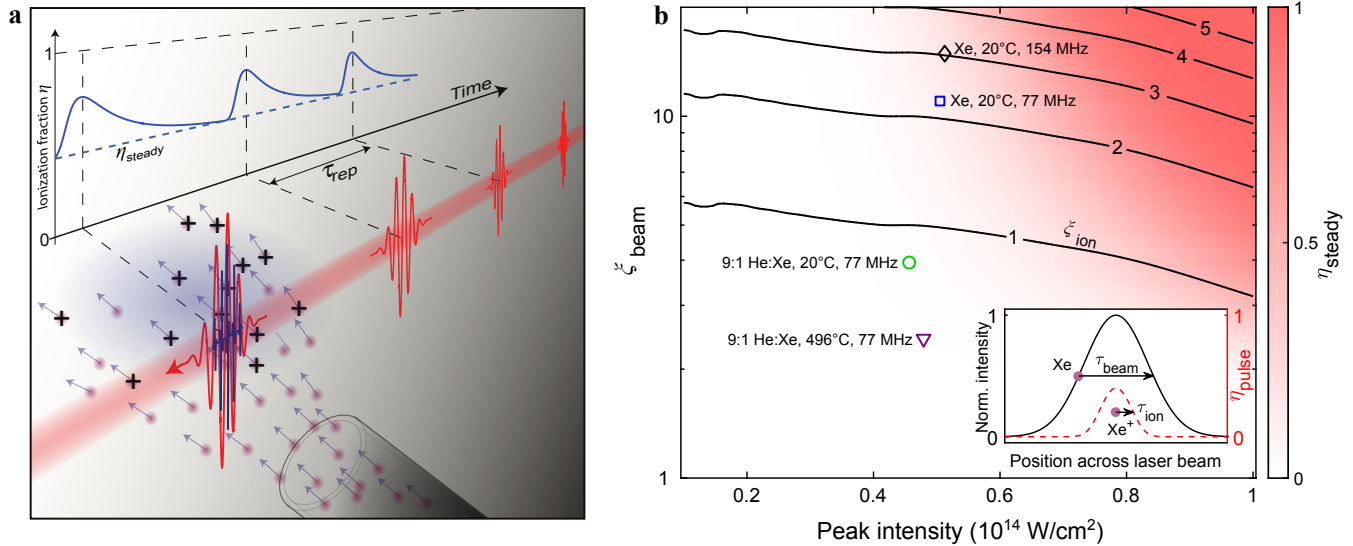


Figure 1: (a) Overview of plasma dynamics in high-repetition-rate high-harmonic generation. A train of femtosecond laser pulses crosses and ionizes a xenon gas jet. The interval between consecutive pulses, $\tau_{\text{rep}} = 1/f_{\text{rep}}$, is smaller than the plasma transit time through the ionization volume, resulting in a high steady-state ionization fraction, η_{steady} . (b) Spatially-averaged steady-state ionization fraction, η_{steady} (colour scale), as a function of peak laser intensity and the number of laser pulses that cross the gas jet during the gas transit time through the laser beam, $\xi_{\text{beam}} = \tau_{\text{beam}}/\tau_{\text{rep}}$. The contour lines show the intensity-dependent number of laser pulses $\xi_{\text{ion}} = \tau_{\text{ion}}/\tau_{\text{rep}}$ that cross the gas jet during the time it takes an ion to clear the ion-generation volume, as illustrated in the inset. The black diamond ($\eta_{\text{steady}} = 17\%$), blue square ($\eta_{\text{steady}} = 11\%$), green circle ($\eta_{\text{steady}} = 1.1\%$), and purple triangle ($\eta_{\text{steady}} = 0.2\%$), indicate experimental conditions of optimal 11th harmonic yield for various gas and laser parameters.

$\xi_{\text{ion}} = \tau_{\text{ion}}/\tau_{\text{rep}}$, where τ_{ion} is the transit time of an ion through the half-width at half-maximum (HWHM) of the intensity-dependent ion-generation volume. This volume is defined by the ionization probability profile created by a single laser pulse, $\eta_{\text{pulse}}(x)$, which is calculated numerically (see Methods). Similarly, $\xi_{\text{beam}} = \tau_{\text{beam}}/\tau_{\text{rep}}$, where $\tau_{\text{beam}} = \sigma_{\text{FWHM}}/v_{\text{gas}}$. Here, σ_{FWHM} is the full-width at half-maximum (FWHM) of the intensity profile and $v_{\text{gas}} = \sqrt{5RT/M_{\text{avg}}}$ is the translational velocity of the gas³⁷ perpendicular to the laser propagation direction, with R denoting the universal gas constant, T the gas stagnation (backing) temperature, and M_{avg} the weighted-average molar mass of the monatomic gas mixture.

The steady-state ionization fraction η_{steady} (spatially-averaged over the intensity profile) is shown in Figure 1b as a function of ξ_{beam} and laser intensity, where the contour lines correspond to ξ_{ion} . The HHG yield from a single atom increases with intensity, however, Fig. 1b shows that higher intensity also corresponds to higher steady-state ionization fraction. For a fixed intensity, η_{steady} increases with a higher repetition rate or slower gas jet. We note that decreasing the spot size at fixed peak intensity would also decrease the steady-state ionization, however, it would reduce the size of the generation volume, thus preventing a gain in the total harmonic yield.

The ionization fraction is linked to the phase-matching conditions, thus determining directly the XUV yield. In HHG, the phase mismatch is usually expressed as a wave-vector mismatch^{5,6,38}:

$$\Delta k \approx \rho \left((1 - \eta) \left| \frac{\partial \Delta k_n}{\partial \rho_n} \right| - \eta \left| \frac{\partial \Delta k_p}{\partial \rho_p} \right| \right) - |\Delta k_g|. \quad (1)$$

Here, ρ , ρ_n , and ρ_p are the total, neutral, and plasma densities, respectively, η is the ionization fraction, Δk_n and Δk_p are the wave-vector mismatches due to neutral and plasma dispersion, respectively, and Δk_g is the geometric wave-vector mismatch due to the Gouy phase dispersion. Δk_g and $\partial \Delta k_{n,p}/\partial \rho_{n,p}$ are independent of $\rho_{n,p}$. We have not included the intensity-dependent dipole phase contribution to Δk , as it is negligible in our conditions where the generation medium is much shorter than the Rayleigh length of the generating beam³⁹. An optimum harmonic yield is reached for $\Delta k = 0$, corresponding to an infinite coherence length $L_{\text{coh}} = \pi/\Delta k$. From Eq. (1) we see that the neutral and plasma dispersion can compensate the Gouy phase shift for a certain gas density, but only if the ionization fraction stays below a critical value. As the HHG radiation is absorbed by the generation medium, the effective coherence length is limited, therefore the maximum yield is absorption-limited. A simplified 1D analysis⁵ shows that, for a given absorption

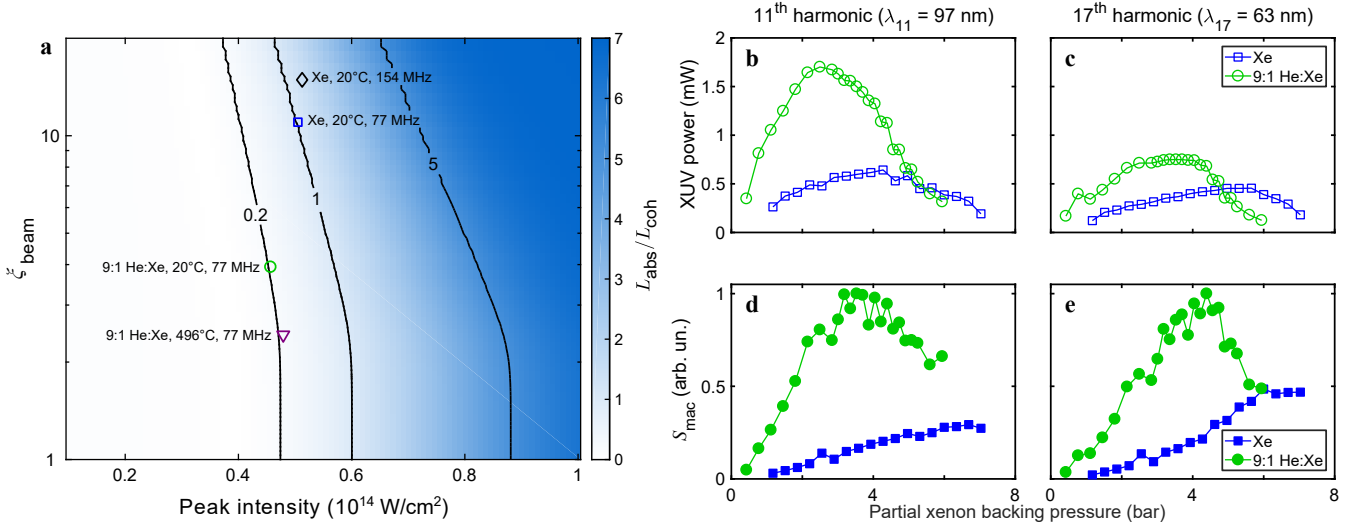


Figure 2: (a) Spatially-averaged phase-matching figure-of-merit at the peak of the laser pulse, $L_{\text{abs}}/L_{\text{coh}}$ (colour scale and contour line), for the 11th harmonic, as a function of peak laser intensity and ξ_{beam} . Phase matching requires $L_{\text{abs}}/L_{\text{coh}} \lesssim 0.2$. The markers correspond to the same experimental conditions as displayed in Fig. 1b. (b) and (c) Measured 11th and 17th harmonic power versus partial xenon backing pressure. (d) and (e) The macroscopic response S_{mac} , which is the measured harmonic power divided by the measured single-atom response. The overturning peaks in the 9:1 He:Xe gas mix curves in figures (d) and (e) indicate phase matching.

length, the harmonic yield will reach at least half of its optimum when the coherence length is sufficiently long such that $L_{\text{abs}}/L_{\text{coh}} \leq 0.2$, where $L_{\text{abs}} = (\sigma \rho)^{-1}$ is the absorption length with absorption cross section σ . Since HHG is a highly-nonlinear process, phase-matching is most important near the peak of the laser pulse. Figure 2a shows spatially-averaged $L_{\text{abs}}/L_{\text{coh}}$ at the peak of the pulse, simulated for the 11th harmonic ($\lambda_{11} = 97$ nm) under our experimental conditions (see Methods), on the same axes as those used to display the steady-state ionization fraction in Fig. 1b. The expected trend of improved phase matching with lower steady-state ionization, which is reached for faster gas jet velocities and lower intensities, is clearly visible.

Plasma accumulation would be avoided in the single pulse regime, $\xi_{\text{ion}} \leq 1$, when a significant part of the plasma clears the generation volume between consecutive pulses. This has not been the case for previous HHG work at $f_{\text{rep}} \gg 10$ MHz. In order to achieve single-pulse conditions in our experiment, we increase the gas velocity by increasing its temperature or by seeding the heavy generator gas (Xe) in a light carrier gas (He) (i.e., decreasing M_{avg})^{11,32,37}. Under our experimental conditions (77 MHz, focal spot size $\sigma_{\text{FWHM}} = 41$ μm , $I_{\text{peak}} \approx 5 \times 10^{13}$ W/cm²) we expect to transition into the single pulse regime when the helium fraction is about 80%, corresponding to a gas speed of 648 m/s (compared to 305 m/s for pure Xe) at room temperature (see Figs. 1b and 2a). The ionization potential of He (24.6 eV) is much higher than that of Xe (12.13 eV), thus at our laser intensity,

helium does not contribute to XUV emission and does not add any more plasma. We note that He dispersion is comparable to Xe dispersion in a 9:1 He:Xe gas mix, and XUV absorption in He is negligible for harmonic orders ≤ 21 .

We perform HHG in an enhancement cavity (see Fig. 1 in Ref. 12), where the driving laser power is enhanced by a factor of ~ 200 at repetition rates of 154 MHz or 77 MHz via pulse picking (see Methods for details). Reducing the plasma level in the HHG generation volume comes with additional benefits for intracavity HHG. In an enhancement cavity, the plasma's dispersion limits the power build-up in the cavity, thus restricting the focus intensity^{8,9,32}. The dependence of η_{steady} on laser intensity causes optical bistability and coupling to higher order transverse modes due to plasma lensing, which also limit the intracavity focal intensity^{7-9,11}.

Figures 2b and 2c show the experimentally generated power S_q of the harmonic order $q = 11$ and 17 ($\lambda_{17} = 63$ nm), as a function of partial xenon backing pressure, for the case of a pure xenon jet and a 9:1 He:Xe gas mixture. Increasing the gas density increases the dispersive and nonlinear effects of the plasma in the enhancement cavity^{8,9,32}, leading to a decreased intracavity intensity I as the backing pressure is increased. In order to remove the ambiguity between the effects of phase matching and intracavity intensity on harmonic yield, we measured the nonlinear intensity-dependence of the single atom response I^{Nq} for each of the two harmonics (see Methods for details). In Figs. 2d and 2e we plot the harmonic power divided by the

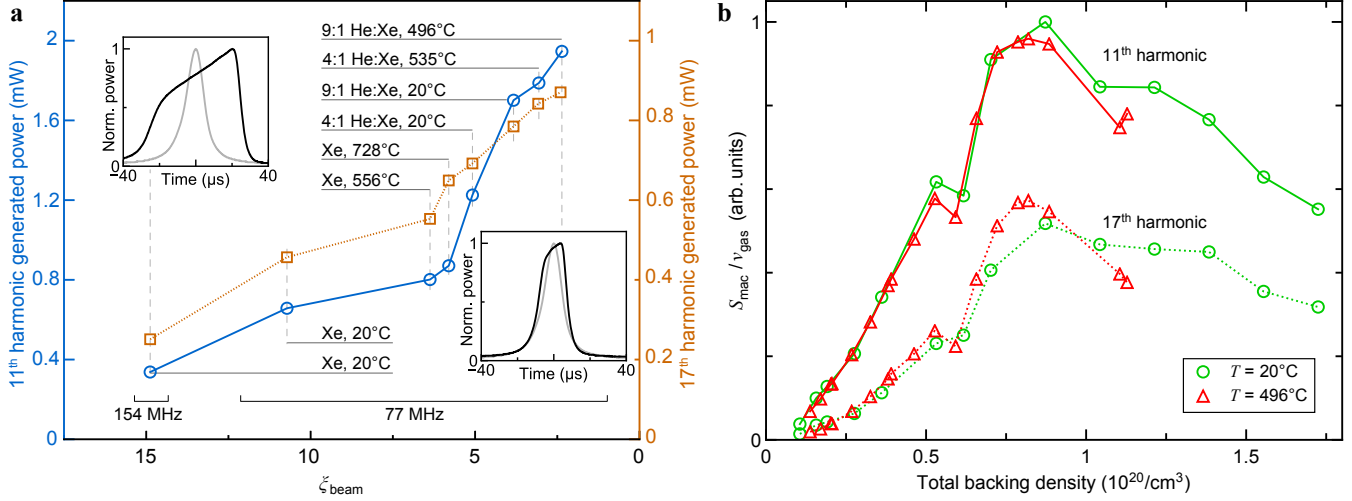


Figure 3: (a) Experimentally generated 11th and 17th harmonic power as a function of ξ_{beam} for experimental conditions with different repetition rates, gas mixes, and gas temperatures. Each point corresponds to the peak of a pressure-curve analogous to Fig. 2b and 2c. The insets show intracavity laser power while sweeping over the cavity resonance with gas (black) and without gas (grey) for the smallest and largest ξ_{beam} . (b) Pressure scan of the macroscopic response S_{mac} scaled by the calculated gas terminal velocity v_{gas} for the 9:1 He:Xe gas mixture with the nozzle unheated (20°C) and heated (estimated gas temperature $\sim 496^\circ\text{C}$). The horizontal axis is transformed from pressure and temperature to density assuming ideal gas behaviour.

single atom response, $S_{q,\text{mac}} = S_q / I^{N_q}$, thus we remove the effect of the variation in generating intensity. For each of the two harmonics, we observe a clear peak for the case of the gas mix, as expected for phase-matched and absorption-limited generation [see Eq. (1)], while for pure xenon we obtain a saturation behaviour with no discernible peak. These results indicate that phase matching is reached when the gas mix is used.

There are three other effects that could explain a peak in S_{mac} as a function of pressure, which are excluded in our experiment. First, absorption of the generated harmonics behind the generation medium. This can be excluded as the chamber background pressure is kept below 2×10^{-2} mbar, and the Rayleigh length is much greater than the effective medium length defined by the gas distribution. Second, a possible reshaping of the laser pulse upon propagation through the nonlinear medium would depend on the gas density and could cause unfavourable phase matching at high densities. However, significant reshaping effects would also affect the harmonics generated with pure Xe. Third, clustering at high densities could influence the HHG process. In order to exclude effects due to clustering, we heated our nozzle to 560°C , leading to estimated gas temperatures of $\sim 496^\circ\text{C}$ for the 9:1 He:Xe mixture. This corresponds to a $\sim 1.6\times$ higher gas jet speed due to heating. We note that we empirically observed a linear scaling of the HHG yield with gas jet speed when $\xi_{\text{beam}} < 6$ (see Fig. 3a). In this range the steady-state plasma is mostly, but not completely,

avoided, so increasing the gas jet speed still gradually reduces the steady-state plasma. The effect of this η_{steady} reduction on harmonic yield can thus be modelled with a first order approximation, i.e., a linear scaling. It is important to note that this scaling does not affect any conclusions regarding the macroscopic generation conditions, since a change in the macroscopic conditions would change the harmonic yield dependence on density, not just the overall level. The measured harmonic power scaled according to the single atom response and the gas jet terminal velocity, $S_{q,\text{mac}}/v_{\text{gas}}$, is shown in Fig. 3b as a function of the backing gas density, for both the unheated and heated nozzle case with 9:1 He:Xe gas mix. The two data sets match very well, showing that in both cases the dispersion and absorption properties of the generating medium conditions are the same. This indicates that cluster formation, which is strongly dependent on temperature⁴⁰, does not play a role here. This conclusion is also supported by a recent investigation of xenon clustering in HHG, in which such effects were only observed at a large distance from the nozzle where the clusters contain at least 10^4 atoms⁴¹, while here we perform HHG within 1–2 nozzle diameters from the orifice.

We experimentally studied the dependence of generated harmonic power on ξ_{beam} , using different gas mixes and temperatures, displayed in Fig. 3a. Both the 11th and 17th harmonic power monotonically increase as ξ_{beam} decreases. For both harmonics, the power increases with a roughly-constant slope as ξ_{beam} is reduced to ~ 6 . This trend stems

from the increased number of neutral xenon atoms available for HHG and a slight improvement of phase matching. Beyond this point, the slope increases dramatically. We attribute this dramatic increase to the onset of significant phase matching due to the transition into the single-pulse regime. Indeed, as seen in Fig. 1b, $\xi_{\text{beam}} \approx 6$ corresponds to $\xi_{\text{ion}} \approx 1$. As explained above, the continued gradual reduction of the steady-state plasma is the reason the measured harmonic yield does not saturate. Another indication that the steady-state plasma is decreasing is the mitigation of plasma-induced cavity bistability⁷⁻⁹ for lower ξ_{beam} , indicated by the narrower and nearly Lorentzian intracavity power curve measured by sweeping the cavity length, shown in the insets of Fig. 3a. To connect the experimental results of Fig. 3a with our calculation of steady-state ionization and phase matching, we placed markers on Figs. 1b and 2a, which correspond to pressure-optimized 11th-harmonic conditions for various f_{rep} , v_{gas} , and σ_{FWHM} . Fig 1b shows that in the cases of a pure xenon generation medium and either 154 MHz or 77 MHz repetition rate, the single pulse regime is not reached, as opposed to a 9:1 He:Xe gas mix at 77 MHz repetition rate at room temperature and heated. Correspondingly, Fig. 2a predicts a significant improvement in phase matching for the 11th harmonic for the last two cases, as corroborated by the experimental results in Figs. 2d and 3a. Finally, we point out the fact that for the highest gas speeds we have achieved record power levels of ~ 2 mW and ~ 0.9 mW for the 11th and 17th harmonic, respectively (see Fig. 4). These correspond to intracavity conversion efficiencies of 1.8×10^{-7} and 8.5×10^{-8} , which are comparable to those obtained with single-pass phase-matched HHG using a similar generating wavelength at $f_{\text{rep}} = 10.7$ MHz²⁹.

In conclusion, we have demonstrated phase-matched high repetition rate ($\gg 10$ MHz) HHG for the first time, achieving beyond mW power levels per harmonic order, bringing the generated XUV brightness to a similar level obtained from synchrotron sources⁸. Our results not only set a new power record for HHG-based XUV sources in general (including low-repetition rate systems), they also open the door to direct frequency comb spectroscopy in few-electron systems such as He¹⁵ and highly charged ions⁴². We have shown that steady-state plasma mitigation is possible and critical for phase-matching high repetition rate HHG, and that a simple model of plasma motion is sufficient to capture all of the important dynamics involved in plasma accumulation and predict the conditions required for phase matching. The universal physical insight we provide will be indispensable for phase matching and power scaling HHG driven by emerging laser technology with shorter pulses, higher repetition rate and higher power.

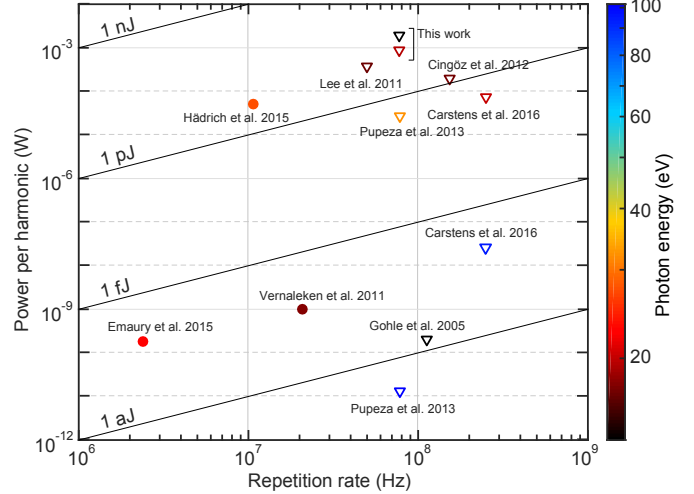


Figure 4: Overview of experimentally generated power per harmonic above 10 eV at repetition rates above 1 MHz, in single-pass configuration (circles)^{28,29,31} and intracavity configuration (triangles)^{10,12,32,33,35}. The photon energy is indicated by marker colour. For the cases where the cavity out-coupling efficiency was not reported, we assume 10% and 5% for Brewster plate out-coupler¹⁰ and hole mirror³², respectively.

Methods

Experimental Apparatus

The main experimental system is described in detail elsewhere^{4,12}; here we provide a brief overview. The laser is a Yb:fibre amplified frequency comb delivering 120 fs pulses, spectrally centred at 1070 nm⁴³. By optionally inserting an electro-optic pulse picker before the final fibre amplifier stage, we operate with an amplifier-saturated output power of 80 W at either $f_{\text{rep}} = 154$ MHz or 77 MHz. The 3.9 m roundtrip ring cavity (single-pulse resonant for 77 MHz; two-pulse resonant for 154 MHz) is found to give the same HHG performance at 154 MHz as a 1.54 m roundtrip cavity (single-pulse resonant for 154 MHz) with the same finesse and focal spot size. In order to maintain the same peak intensity at the same average power for both repetition rates, the cavity is operated with a focal spot size of $\sigma_{\text{FWHM}} = 29 \mu\text{m}$ at $f_{\text{rep}} = 154$ MHz, and this is increased by $\sqrt{2}$ to $\sigma_{\text{FWHM}} = 41 \mu\text{m}$ at $f_{\text{rep}} = 77$ MHz. The focal spot size is determined experimentally from the frequency spacing of cavity-swept high-order modes⁴⁴. The gas jet is injected into the cavity focus with a home-made⁴⁵ fused-silica nozzle with a 36 mm temperature-controlled section wrapped in resistive heater wire, followed by a 50 μm diameter orifice at the tip. Differential gas pumping is maintained by a 1.5 mm diameter orifice gas-catch assembly placed at a distance of ~ 0.5 mm from the nozzle orifice.

The generated XUV harmonics are outcoupled from the cavity by a flat mirror with a nano-etched surface⁴⁶ which acts as a grating for the XUV with an outcoupling efficiency of 6.55% and 10.52% for the 11th and 17th harmonics, respectively, calculated from the groove depth and period measured with an atomic-force microscope. The two selected harmonics are each directed to their detectors via one grazing-incidence reflection on bare-gold mirrors. The 11th harmonic is measured with a NIST-calibrated Al₂O₃ windowless photoemissive detector⁴⁷, and the 17th harmonic is measured using an aluminium-foil-coated silicon photodiode (Opto Diode AXUV100AI). The Si photodiode is calibrated against the NIST photoemissive detector by measuring the 17th harmonic power with both detectors sequentially, under easily-repeatable conditions (unheated pure Xe). We estimate the upper bound of the uncertainty in the generated harmonic power measurement to be $\pm 7\%$. All measurements reported in this article were taken while sweeping the cavity length across its resonance at a rate much slower than the cavity lifetime.

Ionization and Phase-matching Theory

The theoretical ionization fraction is calculated using the modified PPT (Perelomov-Popov-Terent'ev) ionization model⁴⁸. The ionization probability during a single laser pulse is $\eta_{\text{pulse}}(x, t) = 1 - \exp\left[-\int_{-\tau_{\text{rep}}/2}^t w(x, t') dt'\right]$, where $w(x, t)$ is the PPT ionization rate. Correspondingly, the single-pulse ionization probability profile is $\eta_{\text{pulse}}(x) = \eta_{\text{pulse}}(x, \tau_{\text{rep}}/2)$.

The total ionization fraction at position x along the gas propagation direction, and time t during the laser pulse, is calculated as:

$$\eta(x, t) = \eta_{\text{steady}}(x) + [1 - \eta_{\text{steady}}(x)] \eta_{\text{pulse}}(x, t), \quad (2)$$

where $\eta_{\text{steady}}(x)$ is the steady-state ionization fraction built up by all previous pulses, and $[1 - \eta_{\text{steady}}(x)]$ is the steady-state neutral fraction. The steady-state ionization fraction is found by starting with $\eta_{\text{steady}}(x) = 0$ and recursively solving Eq. (2) after shifting the ionization profile spatially by $v_{\text{gas}} \tau_{\text{rep}}$ for each repetition period. The calculation neglects plasma recombination and diffusion, i.e., it assumes that the dominant mechanism determining pulse-to-pulse plasma survival in the focal volume is the forward motion of the plasma in the gas jet. Inaccuracies in the PPT model and the effect of spatial averaging are taken into account, as explained in the next section. As a result, the spatially-averaged steady-state ionization fraction is presented in colour scale in Fig. 1b.

The neutral-atom absorption and dispersion optical constants used in the calculation of $L_{\text{abs}}/L_{\text{coh}}$ in Fig. 2a are taken from refs.^{49–51}. The coherence length is calculated

using Eq. (1), and η is taken as the spatially-averaged ionization fraction at the peak of the laser pulse, calculated using Eq. (2). The calculation is performed with $\sigma_{\text{FWHM}} = 41 \mu\text{m}$ focal diameter and 2.4 bar partial xenon backing pressure, which was the optimal experimental pressure for the 11th harmonic with 9:1 He:Xe mixture and close to optimum for the other mixtures. The gas density in the focal volume is taken to be 10% of the backing density, which is a reasonable estimation for generation within 1–2 nozzle diameters of the nozzle exit^{9,37}. As the neutral phase mismatch depends on the gas mixing ratio, and the Gouy phase mismatch depends on focal spot diameter, the black diamond and blue square markers in Fig. 2, representing data taken at 154 MHz and 77 MHz with pure xenon, respectively, do not correspond to the same phase-matching conditions as the other markers. Therefore, the calculated $L_{\text{abs}}/L_{\text{coh}}$ differ by 6% and 11%, respectively, from the displayed colour scale value. However, for completeness and as the error is small, we choose to include the markers.

Single-Atom Intensity Dependence and Ionization Model

We measure the intensity-dependence of the single-atom response by continuously monitoring the intracavity power by leakage through a cavity mirror, and scanning the cavity input power while measuring the harmonic power for an extremely-low gas pressure. In particular, we use an unheated 4:1 He:Xe gas mix and a 9:1 He:Xe gas mix with ~ 860 mbar total backing pressure. In these low-density conditions, absorption is negligible and Δk is dominated by the Gouy phase mismatch [see Eq. (1)], so that phase matching is independent of intracavity power (or intensity). Furthermore, the low gas density makes the impact of dispersion and plasma dynamics on the cavity performance negligible. To determine the intensity-dependence of the single-atom response⁵², I^{N_q} , with $N_q < q$ for high-harmonic order q , we fit the low intensity part of the scan, where $\eta \ll 1$, using N_q as a fitting parameter. We find $N_{11} = 4.43(7)$ and $N_{17} = 4.75(11)$, respectively, in agreement with past results⁵².

The PPT ionization model is known to provide the correct trend but not the correct magnitude of the ionization rate⁴⁸. Additionally, we want to account for the effect of spatial averaging. Therefore, we use the high-intensity part of the scan, which deviates from the I^{N_q} power law due to significant neutral depletion, in order to fit a multiplicative factor to the PPT ionization rate. The harmonic signal is fitted to the temporally-integrated product $I^{N_q} (1 - \eta)^2$ (using the values of N_q obtained from the low intensity scan), resulting in a global multiplicative fitting factor of 0.52(4) for $w(x, t)$. This fitting factor effectively accounts for PPT inaccuracies, spatial averaging, and the systematic error in the measured intensity (estimated to be at most 20%).

References

- [1] A. McPherson, G. Gibson, H. Jara, U. Johann, T. S. Luk, I. a. McIntyre, K. Boyer, and C. K. Rhodes, "Studies of multiphoton production of vacuum-ultraviolet radiation in the rare gases," *J. Opt. Soc. Am. B* **4**, 595 (1987).
- [2] M. Ferray, A. L'Huillier, X. F. Li, L. A. Lompré, G. Mainfray, and C. Manus, "Multiple-harmonic conversion of 1064 nm radiation in rare gases," *J. Phys. B: At., Mol. Opt. Phys.* **21**, L31 (1988).
- [3] R. A. Bartels, A. Paul, H. Green, H. C. Kapteyn, M. M. Murnane, S. Backus, I. P. Christov, Y. Liu, D. Atwood, and C. Jacobsen, "Generation of Spatially Coherent Light at Extreme Ultraviolet Wavelengths," *Science* **297**, 376 (2002).
- [4] C. Benko, T. K. Allison, A. Cingöz, L. Hua, F. Labaye, D. C. Yost, and J. Ye, "Extreme ultraviolet radiation with coherence time greater than 1 s," *Nature Photon.* **8**, 530 (2014).
- [5] E. Constant, D. Garzella, P. Breger, E. Mével, C. Dorrer, C. Le Blanc, F. Salin, and P. Agostini, "Optimizing High Harmonic Generation in Absorbing Gases: Model and Experiment," *Phys. Rev. Lett.* **82**, 1668 (1999).
- [6] A. Paul, E. A. Gibson, X. Zhang, A. Lytle, T. Popmintchev, X. Zhou, M. M. Murnane, I. P. Christov, and H. C. Kapteyn, "Phase-matching techniques for coherent soft x-ray generation," *IEEE J. Quantum Electron.* **42**, 14 (2006).
- [7] D. C. Yost, A. Cingöz, T. K. Allison, A. Ruehl, M. E. Fermann, I. Hartl, and J. Ye, "Power optimization of XUV frequency combs for spectroscopy applications [Invited]," *Opt. Express* **19**, 23483 (2011).
- [8] T. K. Allison, A. Cingöz, D. C. Yost, and J. Ye, "Extreme nonlinear optics in a femtosecond enhancement cavity," *Phys. Rev. Lett.* **107**, 1 (2011).
- [9] D. R. Carlson, J. Lee, J. Mongelli, E. M. Wright, and R. J. Jones, "Intracavity ionization and pulse formation in femtosecond enhancement cavities." *Opt. Lett.* **36**, 2991 (2011).
- [10] J. Lee, D. R. Carlson, and R. J. Jones, "Optimizing intracavity high harmonic generation for XUV fs frequency combs," *Opt. Express* **19**, 23315 (2011).
- [11] A. K. Mills, T. J. Hammond, M. H. C. Lam, and D. J. Jones, "XUV frequency combs via femtosecond enhancement cavities," *J. Phys. B: At., Mol. Opt. Phys.* **45**, 142001 (2012).
- [12] A. Cingöz, D. C. Yost, T. K. Allison, A. Ruehl, M. E. Fermann, I. Hartl, and J. Ye, "Direct frequency comb spectroscopy in the extreme ultraviolet," *Nature* **482**, 68 (2012).
- [13] D. Z. Kandula, C. Gohle, T. J. Pinkert, W. Ubachs, and K. S. E. Eikema, "Extreme Ultraviolet Frequency Comb Metrology," *Phys. Rev. Lett.* **105**, 063001 (2010).
- [14] G. W. F. Drake and Z.-C. Yan, "High-precision spectroscopy as a test of quantum electrodynamics in light atomic systems," *Can. J. Phys.* **86**, 45 (2008).
- [15] E. E. Eyler, D. E. Chieda, M. C. Stowe, M. J. Thorpe, T. R. Schibli, and J. Ye, "Prospects for precision measurements of atomic helium using direct frequency comb spectroscopy," *Eur. Phys. J. D* **48**, 43 (2008).
- [16] M. Herrmann, M. Haas, U. D. Jentschura, F. Kottmann, D. Leibfried, G. Saathoff, C. Gohle, A. Ozawa, V. Batteiger, S. Knünz, N. Kolachevsky, H. A. Schüssler, T. W. Hänsch, and T. Udem, "Feasibility of coherent xuv spectroscopy on the 1S-2S transition in singly ionized helium," *Phys. Rev. A* **79**, 1 (2009).
- [17] S. G. Karshenboim, "Precision physics of simple atoms: QED tests, nuclear structure and fundamental constants," *Phys. Rep.* **422**, 1 (2005).
- [18] A. Pálffy, "Nuclear effects in atomic transitions," *Contemp. Phys.* **51**, 471 (2010).
- [19] W. Ubachs, E. J. Salumbides, K. S. E. Eikema, N. De Oliveira, and L. Nahon, "Novel techniques in VUV high-resolution spectroscopy," *J. Electron Spectrosc. Relat. Phenom.* **196**, 159 (2014).
- [20] M. Vogel and W. Quint, "Aspects of fundamental physics in precision spectroscopy of highly charged ions in Penning traps," *Ann. Phys.* **525**, 505 (2013).
- [21] S. Backus, C. G. Durfee, M. M. Murnane, and H. C. Kapteyn, "High power ultrafast lasers," *Rev. Sci. Instrum.* **69**, 1207 (1998).
- [22] C. T. Chiang, A. Blättermann, M. Huth, J. Kirschner, and W. Widdra, "High-order harmonic generation at 4 MHz as a light source for time-of-flight photoemission spectroscopy," *Appl. Phys. Lett.* **101**, 071116 (2012).
- [23] B. Frietsch, R. Carley, K. Döbrich, C. Gahl, M. Teichmann, O. Schwarzkopf, P. Wernet, and M. Weinelt, "A high-order harmonic generation apparatus for time- and angle-resolved photoelectron spectroscopy," *Rev. Sci. Instrum.* **84**, 075106 (2013).

- [24] R. Wallauer, J. Reimann, N. Armbrust, J. Gdde, and U. Hfer, "Intervalley scattering in MoS2 imaged by two-photon photoemission with a high-harmonic probe," *Appl. Phys. Lett.* **109** (2016), 10.1063/1.4965839.
- [25] M. I. Stockman, M. F. Kling, U. Kleineberg, and F. Krausz, "Attosecond nanoplasmonic-field microscope," *Nature Photon.* **1**, 9 (2007).
- [26] R. Drner, V. Mergel, O. Jagutzki, L. Spielberger, J. Ullrich, R. Moshhammer, and H. Schmidt-Bcking, "Cold Target Recoil Ion Momentum Spectroscopy: a 'momentum microscope' to view atomic collision dynamics," *Phys. Rep.* **330**, 95 (2000).
- [27] M. Sabbar, S. Heuser, R. Boge, M. Lucchini, L. Gallmann, C. Cirelli, and U. Keller, "Combining attosecond XUV pulses with coincidence spectroscopy," *Rev. Sci. Instrum.* **85**, 103113 (2014).
- [28] F. Emaury, A. Diebold, C. Saraceno, and U. Keller, "Compact extreme ultraviolet source at megahertz pulse repetition rate with a low-noise ultrafast thin-disk laser oscillator," *Optica* **2**, 980 (2015).
- [29] S. Hdrich, M. Krebs, A. Hoffmann, A. Klenke, J. Rothhardt, J. Limpert, and A. Tnnermann, "Exploring new avenues in high repetition rate table-top coherent extreme ultraviolet sources," *Light Sci. Appl.* **4**, e320 (2015).
- [30] J. Rothhardt, S. Hdrich, A. Klenke, S. Demmler, A. Hoffmann, T. Gottschall, T. Eidam, M. Krebs, J. Limpert, and A. Tnnermann, "53 W average power few-cycle fiber laser system generating soft X-rays up to the water window," *Opt. Lett.* **39**, 5224 (2014).
- [31] A. Vernaleken, J. Weitenberg, T. Sartorius, P. Russbldt, W. Schneider, S. Stebbings, M. Kling, P. Hommelhoff, H.-D. Hoffmann, R. Poprawe, F. Krausz, T. Hnsch, and T. Udem, "Single-pass high-harmonic generation at 20.8 MHz repetition rate," *Opt. Lett.* **36**, 3428 (2011).
- [32] H. Carstens, M. Hgner, T. Saule, S. Holzberger, N. Lillienfein, A. Guggenmos, C. Jocher, T. Eidam, D. Esser, V. Tosa, V. Pervak, J. Limpert, A. Tnnermann, U. Kleineberg, F. Krausz, and I. Pupeza, "High-harmonic generation at 250 MHz with photon energies exceeding 100 eV," *Optica* **3**, 366 (2016).
- [33] C. Gohle, T. Udem, M. Herrmann, J. Rauschenberger, R. Holzwarth, H. A. Schuessler, F. Krausz, and T. W. Hnsch, "A frequency comb in the extreme ultraviolet," *Nature* **436**, 234 (2005).
- [34] R. J. Jones, K. D. Moll, M. J. Thorpe, and J. Ye, "Phase-coherent frequency combs in the vacuum ultraviolet via high-harmonic generation inside a femtosecond enhancement cavity," *Phys. Rev. Lett.* **94**, 1 (2005).
- [35] I. Pupeza, S. Holzberger, T. Eidam, H. Carstens, D. Esser, J. Weitenberg, P. Rubldt, J. Rauschenberger, J. Limpert, T. Udem, A. Tnnermann, T. W. Hnsch, A. Apolonski, F. Krausz, and E. Fill, "Compact high-repetition-rate source of coherent 100 eV radiation," *Nature Photon.* **7**, 608 (2013).
- [36] T. Popmintchev, M.-C. Chen, P. Arpin, M. M. Murnane, and H. C. Kapteyn, "The attosecond nonlinear optics of bright coherent X-ray generation," *Nature Photon.* **4**, 822 (2010).
- [37] D. R. Miller, "Free Jet Sources," in *Atomic and Molecular Beam Methods*, Vol. 1, edited by G. Scoles (Oxford University Press, 1988) Chap. 2.
- [38] C. M. Heyl, J. Gdde, A. L'Huillier, and U. Hfer, "High-order harmonic generation with μ J laser pulses at high repetition rates," *J. Phys. B: At., Mol. Opt. Phys.* **45**, 074020 (2012).
- [39] C. M. Heyl, C. L. Arnold, A. Couairon, and A. L'Huillier, "Introduction to macroscopic power scaling principles for high-order harmonic generation," *J. Phys. B: At., Mol. Opt. Phys.* **50**, 13001 (2017).
- [40] J. W. G. Tisch, T. Ditmire, D. J. Fraser, N. Hay, M. B. Mason, E. Springate, J. P. Marangos, and M. H. R. Hutchinson, "Investigation of high-harmonic generation from xenon atom clusters," *J. Phys. B: At., Mol. Opt. Phys.* **30**, L709 (1997).
- [41] N. Li, Y. Bai, P. Peng, R. Li, and Z. Xu, "Electron motion enhanced high harmonic generation in xenon clusters," (2016), [arXiv:1606.01677](https://arxiv.org/abs/1606.01677).
- [42] J. R. Crespo Lpez-Urrutia, "Frequency metrology using highly charged ions," *J. Phys.: Conf. Ser.* **723**, 012052 (2016).
- [43] A. Ruehl, A. Marcinkevicius, M. E. Fermann, and I. Hartl, "80 W, 120 fs Yb-fiber frequency comb." *Opt. Lett.* **35**, 3015 (2010).
- [44] A. E. Siegman, *Lasers* (University Science Books, 1986).
- [45] C. M. Heyl *et al.*, (2017), in preparation.
- [46] D. C. Yost, T. R. Schibli, and J. Ye, "Efficient output coupling of intracavity high-harmonic generation," *Opt. Lett.* **33**, 1099 (2008).

- [47] R. E. Vest, L. R. Canfield, M. L. Furst, R. M. Graves, A. D. Hamilton, L. R. Hughey, T. B. Lucatorto, and R. P. Madden, “NIST programs for calibrations in the far ultraviolet spectral region,” (1999).
- [48] S. F. Zhao, A. T. Le, C. Jin, X. Wang, and C. D. Lin, “Analytical model for calibrating laser intensity in strong-field-ionization experiments,” *Phys. Rev. A* **93**, 1 (2016).
- [49] A. L’Huillier, X. F. Li, and L. A. Lompré, “Propagation effects in high-order harmonic generation in rare gases: errata,” *J. Opt. Soc. Am. B* **7**, 2137 (1990).
- [50] F. M. Masunaga, R. S. Jackson, and K. Watanabe, “Photoionization yield and absorption coefficient of xenon in the region of 860-1022 Angstrom,” *J. Quant. Spectrosc. Radiat. Transfer* **5**, 329 (1965).
- [51] E. A. Reinsch, “Calculation of dynamic polarizabilities of He, H₂, Ne, HF, H₂O, NH₃, and CH₄ with MC-SCF wave functions,” *J. Chem. Phys.* **83**, 5784 (1985).
- [52] A. L’Huillier, P. Balcou, S. Candel, K. J. Schafer, and K. C. Kulander, “Calculations of high-order harmonic-generation processes in xenon at 1064 nm,” *Phys. Rev. A* **46**, 2778 (1992).

Acknowledgements

This work was supported by the Air Force Office of Scientific Research, National Institute of Standards and Technology and the National Science Foundation Physics Frontier Center at JILA (PHY-1734006). C.M.H. was supported by the Swedish Research Council. K.L.C. acknowledges the support of the JILA Visiting Fellows Program.

Author contributions

All authors contributed to the design, planning and execution of the experiment. G.P., C.M.H., S.B.S., C.B., and J.Y. analysed the data. All authors contributed to the writing of the manuscript. G.P., C.M.H., and S.B.S. contributed equally to this work.

Competing financial interests

The authors declare no competing financial interests.